

Damage Survey of Hurricane Andrew and Its Relationship to the Eyewall

Roger M. Wakimoto*
and Peter G. Black†

Abstract

A damage map documenting Hurricane Andrew's destructive landfall over southern Florida is presented. Vectors that represent the direction of winds causing damage to trees and structures are shown along with an F-scale rating in order to assess the strength of the near-surface winds. It is hypothesized that increased surface roughness once the hurricane made landfall may have contributed to a surface wind enhancement resulting in the strongest winds ever estimated (F3) for a landfall hurricane. This intense damage occurred primarily during the "second" period of strong winds associated with the east side of the eyewall. For the first time, a well-defined circulation in the damage pattern by the second wind was documented. A superposition of radar data from Miami and Key West on top of the damage map provides the first detailed examination of the relationship between the eyewall and the surface flow field as estimated from the damage vectors.

1. Introduction

On the morning of 24 August 1992, the eye of Hurricane Andrew made landfall over Dade County, Florida, and continued westward into the Everglades. An infrared satellite image of the hurricane at 0800 UTC (hereafter, all times are UTC) is shown in Fig. 1 when the eye was located just offshore. It was the third strongest hurricane to strike the United States this century (behind Camille and an unnamed 1935 storm that made landfall over the Florida Keys) and, as a result, carved a path of destruction across southern Florida and later into Louisiana, making it the costliest natural disaster in U.S. history (Mayfield and Avila 1993).

In response to a request by the Hurricane Research Division, a survey team embarked on two separate trips to the devastated area to assess the wind effects using aerial and ground surveying techniques dis-

cussed by Fujita et al. (1976) and Fujita (1981, 1992). These types of surveys, originally developed for poststorm surveys of tornadoes, have proven to be particularly useful in defining the surface wind field during the landfall of a hurricane based on the direction of tree fall and structural damage (e.g., Fujita 1980; Fujita et al. 1980). It also provides an indirect estimate of the peak wind speeds accompanying the hurricane by use of the F scale (Fujita 1981).

Although the effect of friction on hurricanes at landfall has been studied by several investigators (e.g., Hubert 1955; Miller 1964; Tuleya and Kurihara 1978; and Tuleya et al. 1984), Shapiro (1983) notes that detailed observations of asymmetries in the boundary layer of hurricanes are very limited. Powell (1982) assembled perhaps the most complete composite surface analysis over the ocean and during landfall using numerous aircraft, ship, buoy, and land station reports.

The first documented reports of hurricane structure as recorded by a radar were by Maynard (1945) and

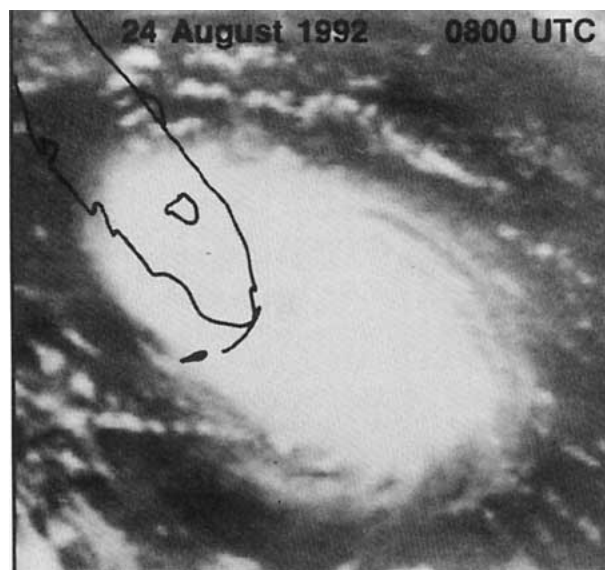


Fig. 1. Infrared satellite image of the cloud shield associated with Hurricane Andrew at 0800 UTC 24 August 1992.

*Department of Atmospheric Sciences, UCLA, Los Angeles, California
†NOAA, Hurricane Research Division, Miami, Florida
In final form 10 September 1993.

Corresponding author address: Roger M. Wakimoto, University of California, Los Angeles, Department of Atmospheric Sciences, 405 Hilgard Avenue, Los Angeles, CA 90024-1565.

©1994 American Meteorological Society

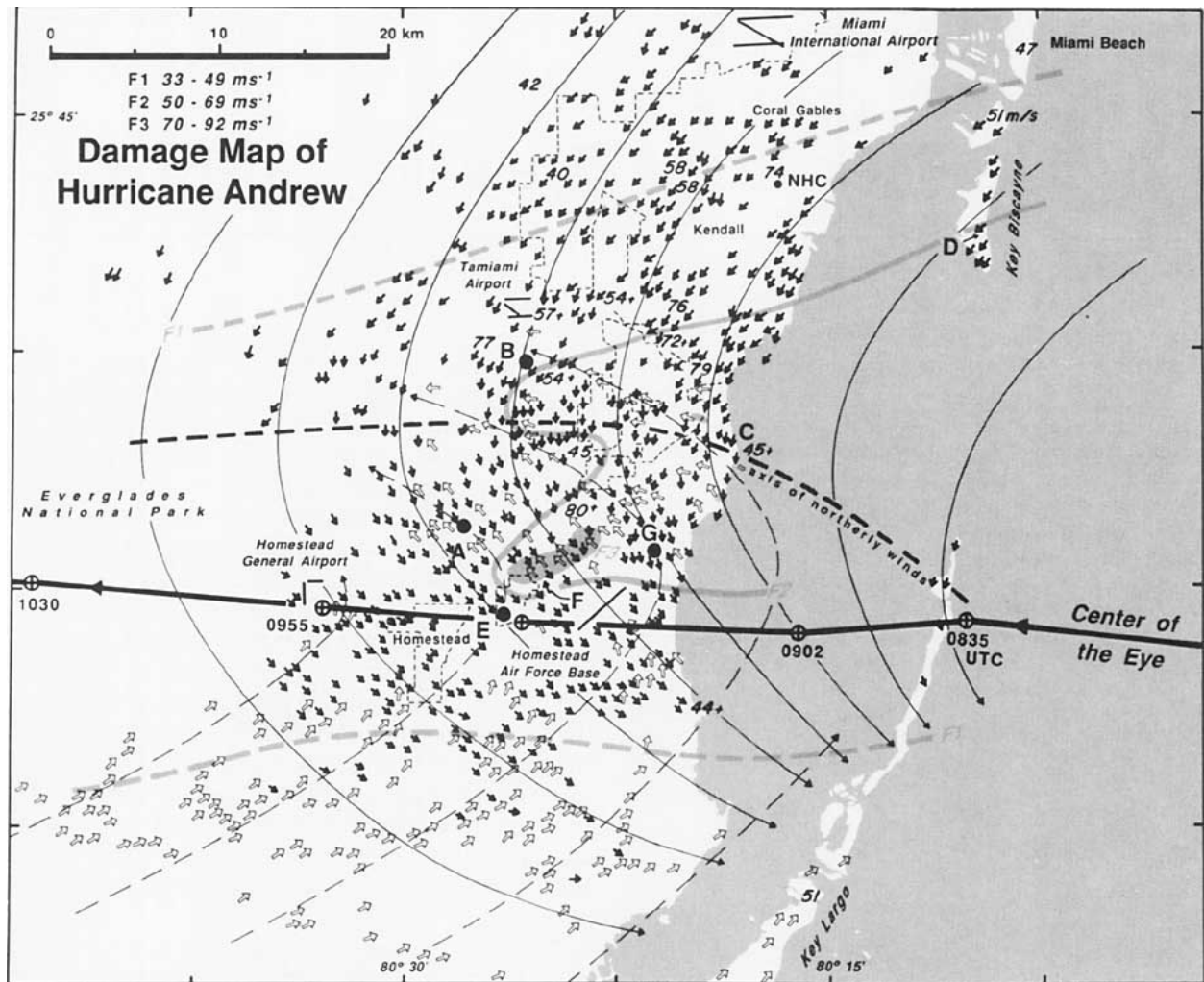


FIG. 2. Damage map of Hurricane Andrew. The arrows represent vectors of tree and structural damage. The black and white arrows represent "first" and "second" wind effects, respectively. Approximate streamlines of these two flow fields (black lines—first wind, black dashed lines—second wind) are drawn on the figure. F-scale analysis is also indicated. Dashed gray lines, gray lines, and shaded gray represent the boundaries of F1 ($33\text{--}49\text{ m s}^{-1}$), F2 ($50\text{--}69\text{ m s}^{-1}$), and F3 ($70\text{--}92\text{ m s}^{-1}$) damage, respectively. Approximate track of the center of the eye based on radar tracking is shown. Thick black dashed line represents the location of the northerly flow as determined by the damage vectors. Numerical values labeled throughout the map represent recorded wind speed estimates (m s^{-1}) from surface anemometers. Letter labels represent locations where aerial or ground photographs were taken. The black dot labeled NHC ($\approx 10\text{ km}$ west of Key Biscayne) denotes the location of the National Hurricane Center and the WSR-57 radar.

later by Wexler (1947). Maynard (1945) noted that the eye of the storm appeared "as a dark area surrounded by curve bands of echoes." The term "eyewall" was introduced to define the intense convective band surrounding the rain-free eye where the heaviest precipitation occurs (e.g., Anthes 1982; Jorgensen 1984a). Using airborne radar and in situ measurements, Jordan et al. (1960) appear to be the first to show that the strongest wind speeds accompanying a hurricane were near the eyewall, and Jorgensen (1984a,b) determined that the zone of maximum eyewall radar reflectivity was several kilometers radially outward from the radius of maximum winds at low levels. Marks

and Houze (1984, 1987) and Marks et al. (1992) have presented unprecedented finescale information on the kinematic structure within the eyewall of three hurricanes by synthesizing airborne Doppler velocities. All of these studies were primarily based on data collected over the ocean and, as a result, the relationship between the eyewall and the surface winds during landfall has never been clearly documented.

There are two primary goals in this article:

- 1) Compile the results of the aerial and ground surveys to clearly document the path of destruction left behind by Andrew. The resultant map will reveal the gradation of damage over southern Florida based

on the F-scale analysis and also provide an integrated view of the surface peak wind flow pattern.

2) Document the relationship between the surface wind and radar-detected eyewall by superimposing the damage map on top of precisely aligned radar images recorded at Miami and Key West. Such an analysis has only been attempted by Fujita (1980) for Hurricane Celia; however, it was only for a single time and the damage map was not as complete (e.g., no vectors were drawn) as the one in the present study.

Section 2 summarizes the results from the aerial and ground surveys over southern Florida. The relationship between the damage map presented in section 2 and the radar-detected eyewall is shown in section 3. Section 4 discusses the possible reasons why the circulation associated with Andrew appeared to have intensified after landfall, and section 5 presents a summary.

2. Survey results

a. Damage map

Two poststorm surveys over south Florida were conducted on 5–9 September and 3–4 October 1992. In particular, extensive aerial surveys were flown on 5–8 September using Cessna aircraft. The resultant damage map is shown in Fig. 2. The approximate track of the geometric center of the eye based on radar data is shown by the heavy black line. The eye of Andrew propagated westward at 8–8.5 m s⁻¹ south of Miami and Miami Beach. The path as shown in Fig. 2 places the center directly over the cities of Homestead and Leisure City (the latter city is located at label E), Homestead Air Force Base, and Homestead General Airport.

The arrows denote vectors of the direction of tree fall and structural damage that were plotted onto U.S. Geological Survey maps. The black arrows represent flow associated with the west side of the eye (hereafter referred to as the “first wind”) while the white arrows represent the flow associated with the east side of the eye (hereafter referred to as the “second wind”). The short and resilient vegetation over Everglades National Park contributed to the lack of damage vectors on the western side of Fig. 2.

Streamlines¹ of the first and second flow regimes are shown on the figure. The approximate east–west trough lines accompanying these two flow patterns are separated by 10–11 km with the second wind trough located toward the south. Clearly evident in the

¹Caution should be exercised since by definition a streamline is parallel to the instantaneous velocity of the fluid. For this paper, the authors have assumed that it is parallel to the damage vectors.

streamlines is the smaller radius of curvature associated with the second wind. Both of these observations have been documented before for hurricanes over the ocean. Powell (1982) (see his Fig. 6), using composite surface analyses, and Shapiro (1983) (see his Fig. 5c), using a boundary-layer model, have shown that the displacement of the trough lines and a smaller radius of curvature associated with the second wind are characteristic of a translating hurricane.

The assignment of F-scale values shown in Fig. 2 relies on a subjective assessment of structural damage caused by tornadoes and damaging winds using the guidelines established by Fujita (1981). It is known that the uncertainties in wind speed estimates using the F scale are highly dependent on building codes, which results in an increased ability for some structures (based on superior design and construction) to withstand extreme wind events (Minor 1981). The F-scale contours in Fig. 2 were assigned by Gregory Forbes and Roger Wakimoto based on previous survey experience (e.g., Forbes and Wakimoto 1983) and is their best estimate of the peak gusts over areas about 1 km². Given uncertainties in building strength factors such as exposure to the wind and the amount of flying debris that impacted the structure, and the extent of the area that had to be surveyed, this mapping cannot precisely reflect the wind speed that affected individual structures. Indeed, there were instances when the character of the damage pattern was “spotty” in the sense that one building was heavily damaged while neighboring structures were largely spared. A detailed house-to-house assessment that incorporates the effects of different building codes is beyond the scope of this paper.

It should be noted that nearly all structures in the high-damage area were constructed using straps wrapped around trusses and rafters to hold the roof on. Such connections are two to three times stronger than “hurricane clips” (Simpson connectors for high wind-resistant structures) used in most other hurricane-prone zones and more than ten times stronger than standard wood-frame “toenail” construction typical of the Midwest and other continental locations. In addition, the majority of the structures in this area were concrete-block stucco (CBS) with a poured, steel-reinforced concrete tie beam along the top outside wall, in which the “hurricane straps” are embedded. This design has an uplift resistance twice that for connection to wood-frame structures and 20 times that of toenail construction. These types of structures are shown in areas labeled C and F in Fig. 2. Therefore, the wind equivalents of the F scale, derived for standard construction practices in the Midwest, may be underestimated by as much as one F-scale category, as suggested by Fujita (1992).



FIG. 3. Photograph taken looking toward the west ($\approx 240^\circ$) at point A in Fig. 2. The direction of some of the downed trees is highlighted on the figure.

A large fraction of the area traversed by the hurricane eye was rated between F1 and F2 in damage intensity, including the city of Homestead, which dominated much of the media's attention. There were two



FIG. 4. Aerial photograph showing the comparison between mobile homes (completely destroyed) and houses (minor roof damage) at the point labeled B in Fig. 2. This area was rated F2 in damage intensity.



FIG. 5. Aerial photograph of the damage caused by a possible small tornado moving toward the west in the small gray area labeled C in Fig. 2. Black arrows represent the direction of tree fall and structural damage. The first and second wind vectors in this figure were from approximately north-northeast and east-southeast, respectively. The black dashed line highlights the path of the vortex.

areas rated F3 located northwest of Homestead Air Force Base and also a relatively small area west of the label C where a suspected tornado briefly touched down, respectively. This is believed to be the first time that surface wind speeds have been assessed as high as F3 for a landfall hurricane. As will be shown in section 2b, these two locations of intense damage were surprisingly associated with the second wind. This observation appears contrary to the commonly accepted theory that hurricanes decay rapidly after landfall (e.g., Anthes 1982; Holland 1987) and will be examined in section 3. Both the intensity and the well-defined circulation in the damage pattern left behind by the second wind have not been previously documented.

Most of the strongest damage in Fig. 2 was located north of the geometric center of the eye with a strong gradient of damage intensity between the points labeled E and F, a distance of only a couple of kilometers. This type of asymmetry is commonly observed during tornado surveys. The strongest damage typi-

cally occurs on the side of the vortex where translational and rotational effects are in the same direction (Fujita 1981, see his Fig. 18). Other factors, however, contribute to the asymmetry of the tangential winds associated with hurricanes. These include a large effect arising from the superposition of the vortex and environmental wind field in which it is embedded (Holland 1987). In the ground-relative frame of reference, it has been shown that the low-level maximum winds tend to be located in the right-front quadrant relative to the hurricane center and direction of motion (Shea and Gray 1973; Powell 1982; Shapiro 1983; Frank 1984). An exception is Hughes (1952), who claims that the maximum exists in the right-rear quadrant.

Also plotted on the damage map are the anemometer locations and estimates of surface wind speeds that were recorded during landfall. The source of each wind speed estimate is shown in the Appendix. This information is useful but must be viewed with caution for two reasons:

1) Cup anemometers can suffer from overspeeding at the velocities that were recorded during Hurricane Andrew. The 79 m s^{-1} wind speed located northwest of label C on Fig. 2 is the only measurement that was corrected (down from the original estimate of 95 m s^{-1}) by calibrating the anemometer in a wind tunnel.

2) Several wind speed estimates do not represent the maximum speed at a location owing to the inability of the recorder to exceed a certain numerical value. These measurements are denoted by a plus sign after the number.

Even with these limitations listed above, there is good agreement between the anemometer readings and the F-scale analysis shown in Fig. 2.

The black, dashed line on the damage map represents the axis of northerly winds as determined by the vectors. The effect of increased friction during landfall is to reduce the boundary-layer wind speeds, thus allowing air parcels to accelerate in the direction of the inward-directed pressure gradient and increasing the angle at which the flow crosses the isobars. Over the barrier islands north of Key Largo, the axis of the northerly flow is just north of the eye track. Subsequently, the axis slopes $\approx 10 \text{ km}$ toward the north of the eye track to a

point along the coastline near the label C owing to increased surface roughness. This suggests a counterclockwise rotation of the surface winds with time of $\approx 30^\circ\text{--}35^\circ$ in response to increased friction during landfall. Powell (1982) noted an increase in inflow angle (angle between the actual wind and a tangent to a circle passing through the point centered at the storm) of $\approx 15^\circ\text{--}20^\circ$ in the front quadrant of Hurricane Frederic when the eye was first crossing the coastline.

b. Observations at select locations

There were several locations, labeled with letter identifiers in Fig. 2, that were chosen as representative examples of the destruction caused by Hurricane Andrew. Figure 3 is a photograph looking west ($\text{at} \approx 240^\circ$) into a forest at the point labeled A on the damage map.

The picture graphically illustrates the first and second wind effects. Note the downed trees in two diametrically opposed directions. This suggests that an abrupt shift in peak winds occurred at this location rather than a continuous and gradual turning of the winds. It is also possible that there was a comparatively long interval between two distinct wind speed maxima during which weaker winds changed more gradually. A comparison between relatively well constructed houses and mobile homes in an area where the winds were approximately uniform is shown at point B (Fig. 4). This location was rated below F2 in intensity since the roofs were damaged on the homes but were still intact (Fujita 1981), yet the mobile homes were completely leveled.

Point C denotes the small gray area (located $\approx 2 \text{ km}$ toward the west of the letter label) where it is believed that a small but strong (F3) tornado touched down (Fig. 5) and cut a path approximately 600 m long through a

housing complex before dissipating. The black dashed line in Fig. 5 highlights part of the tornado's path and the black arrows represent the direction of tree and structural damage. Note that both the first and second wind effects are shown again by the approximately north-northeast and east-southeast vectors, respectively. Past studies have shown that it is not unusual for tornadoes to be characterized by intense destruction and a narrow path width (Kelly et al. 1978;

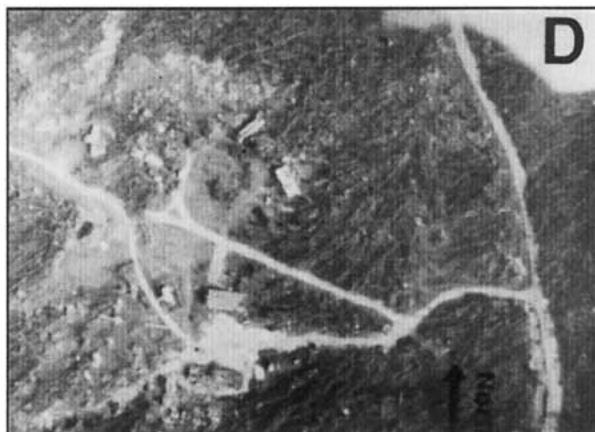


FIG. 6. Aerial photograph taken at point D in Fig. 2. All trees in the southern part of Key Biscayne were blown down toward the southwest.

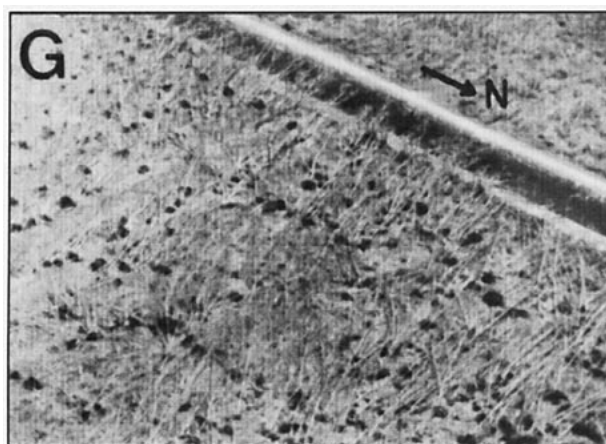


FIG. 7. Aerial photograph taken at point G in Fig. 2. All trees were blown down toward the south-southeast. Exposed roots covered with dirt are clearly seen in the picture.

Wakimoto 1983). The movement of the suspected tornado from east to west, shown in Fig. 5, strongly suggests that it was associated with the second wind or the right-rear quadrant of the hurricane. No other tornado-like vortex was confirmed over the area covered in Fig. 2. Fujita (1993, personal communication) believes that at least 25 similar vortices may have developed in the large gray area denoting the F3 damage intensity.

Tornadogenesis during hurricane landfall has been well documented in the literature (e.g., Orton 1970; Novlan and Gray 1974; Gentry 1983; McCaul 1991). The preferred sector of tornado formation is the right-front quadrant and, to a lesser extent, the right-rear quadrant (Novlan and Gray 1974; McCaul 1991). However, if these data are plotted with respect to the hurricane center and true north, there appears to be a prominent cluster of tornado events in the sector between $\approx 0^\circ$ and 120° (Novlan and Gray 1974; Gentry 1983). McCaul (1991) further subdivides hurricane tornadoes into two apparently distinct regimes—"outer rainband" and "core." The core tornadoes are those that develop near or within the eyewall of the hurricane, and tend to occur mainly during the day of landfall. The Hurricane Andrew tornado shown in Fig. 5 is believed to be the first well-documented case of a core tornado.

Two areas that are representative of damage in excess of F2 are shown in Figs. 6 and 7. The southern part of Key Biscayne marks the northern limit of F2

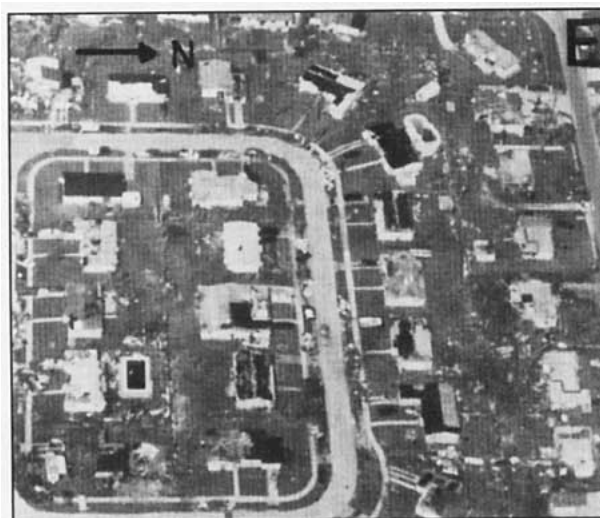


FIG. 8. Aerial photograph taken at point E over Leisure City in Fig. 2. The roofs on the homes are damaged but still remain intact suggesting an F-scale rating between 1 and 2.

damage. Nearly every tree within the aerial photograph shown in Fig. 6 (taken at point D) was blown down toward the southwest. The other location with approximately the same F-scale rating as point D is shown at G (Fig. 7). At this point, trees were stripped and blown down toward the south-southeast. Exposed roots covered with dirt are clearly seen in the picture.



FIG. 9. Photograph of the Naranja Lake area at point F in Fig. 2. Several roofs have been removed and walls have caved in. The black arrows represent the direction of tree damage. Note that the debris from the house in the center of the figure was thrown toward the northwest.

As mentioned in section 2a, there was a remarkable gradient of destruction over a short distance between the points labeled E and F in Fig. 2. An aerial photograph taken over the southern part of Leisure City (point E) is shown in Fig. 8 and is also representative of the type of damage over the city of Homestead. Although the roofs are damaged, they still remain intact (F1–F2) in Fig. 8. However, several kilometers toward the north at point F was the largest area rated F3. An example of an aerial photograph near Naranja Lakes illustrates the destruction of homes with roofs removed and several walls destroyed (Fig. 9). The small black arrows and streamlines represent the direction of tree fall and the scattered debris, respectively. This area is similar to the one shown in Fig. 3 since it illustrates that the first and second wind effects were nearly opposite in direction. It also shows that the F3 damage to the houses was primarily a result of the second wind with the debris being thrown toward the northwest (a ground survey showed that some of the debris over the canal was thrown toward the southeast).

3. Radar analysis

As mentioned previously, the present case study provided a unique opportunity to superimpose the damage map on top of precisely aligned radar images of the eyewall. Complete WSR-57 radar information was recorded on digital tapes (by Hurricane Research

... the winds atop the multistory building reached a force that eventually toppled the [National Hurricane Center] radar antenna from its 3-m pedestal ...

Division personnel) at the National Hurricane Center as Andrew approached southern Florida. A surveillance scan from the Miami radar at 083007 as the eyewall was making landfall is shown in Fig. 10. Unfortunately, the National Hurricane Center was

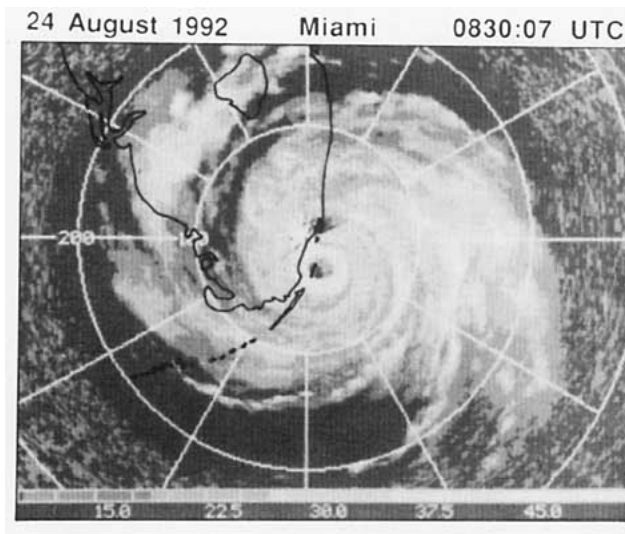
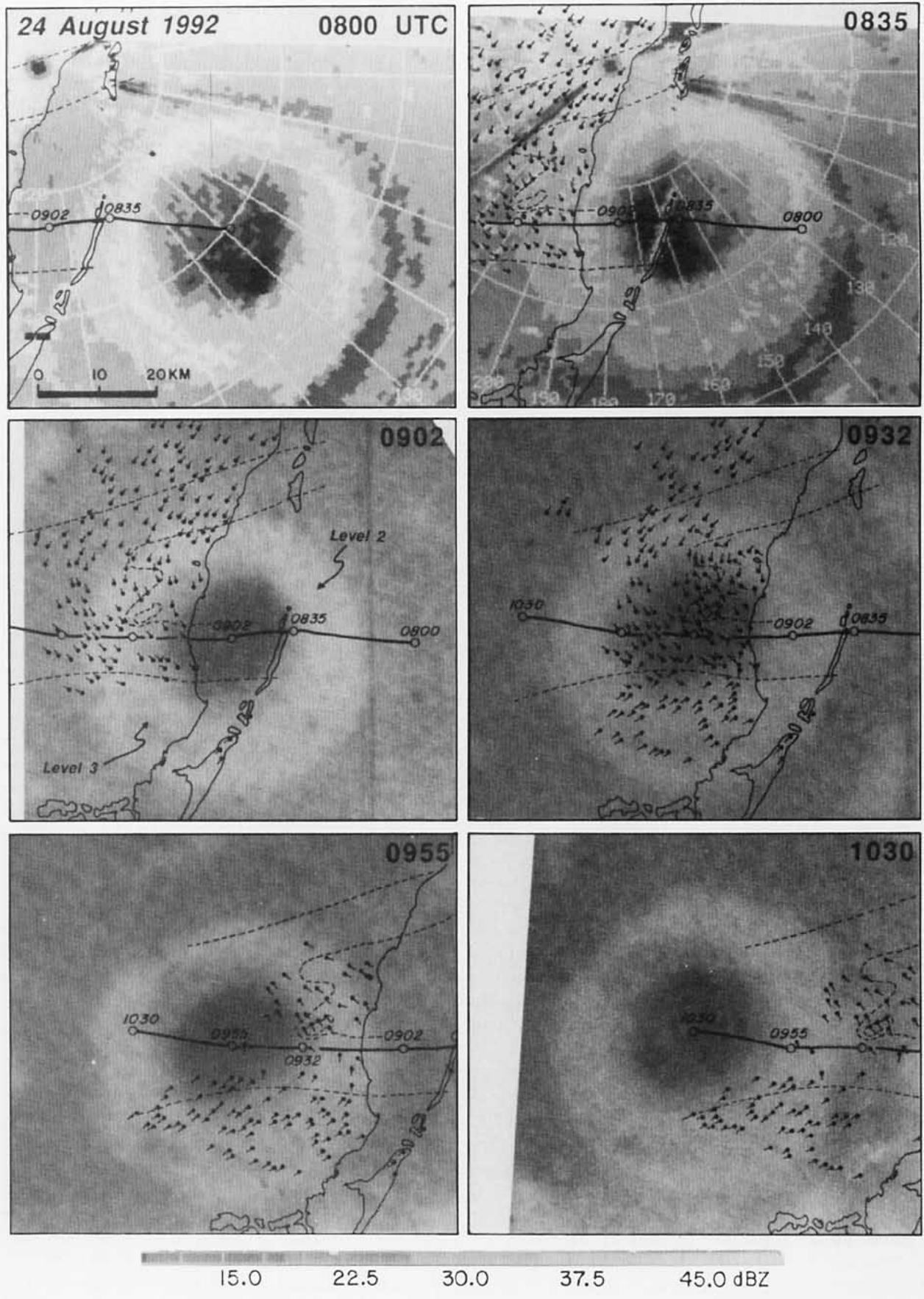


FIG. 10. Surveillance scan of Hurricane Andrew recorded by the Miami radar at 083007 UTC 24 August 1992 as the eyewall was making landfall. The radar reflectivity values are shown by the gray scale in dBZ. Range rings are every 100 km.



FIG. 11. The multistory building that houses the National Hurricane Center. The black arrow denotes the location where the WSR-57 radar was located before the intense winds from Andrew toppled the antenna. The location of the building is shown in Fig. 2.

FIG. 12 (opposing page). Superposition of radar data at 0800, 0835, 0902, 0932, 0955, and 1030 UTC 24 August on top of the coastline, F-scale analysis (dashed lines), and damage vectors. The first two radar images are from the Miami radar, all other images are from the Key West radar. Reflectivity values for the first two images are shown at the bottom of the figure in dBZ. The Key West reflectivity values are shown in Video Integrator and Processor (VIP) levels (level 1—gray, level 2—white, level 3—black) with levels 2 and 3 labeled at 0902. Levels 1, 2, and 3 are approximately equivalent to 30, 36, and 41 dBZ, respectively. Track of the geometric center of the eyewall is also shown.



located within the F1–F2 zone in Fig. 2. Accordingly, the winds atop the multistory building reached a force that eventually toppled the radar antenna from its 3-m pedestal (Fig. 11) a few minutes after the image shown in Fig. 10 [this latter event and other stories are described by Williams (1993)]. Based on the results presented in Fig. 2, it is believed that the Miami radar might have survived intact if it had been located only a few kilometers farther to the north. Radar microfilm from the Key West radar was obtained from the National Climatic Data Center in order to follow the progression of the eyewall after landfall.

The Miami and Key West radar data were subjected to careful ground clutter checks to ensure that the superposition of the eyewall on top of the damage map would contain minimum errors. Subsequently, all radar images were enlarged to the same scale as the damage map. The radar data at 0800, 0835, 0902, 0932, 0955, and 1030 superimposed on top of the coastline, F-scale analysis, and damage vectors are shown in Fig. 12. Note that the island ground clutter north of Key Largo (located in the center of the eye) matches well with the coastline at 0835. The first two images are from the Miami radar; all subsequent images are from the Key West radar. The track of the geometric center of the eyewall is shown by the thick black line. To aid in the interpretation of the results presented in the figure, the vectors have been subjectively plotted at the most likely times when the damage occurred.

The highest reflectivities within the eyewall were initially located approximately in the right-front (north-west) quadrant before landfall and later were noted in the left-front (southwest) quadrant after 0902 in Fig. 12 [note the level three Video Integrator and Processor (VIP) echoes in the left-front quadrant beginning at 0902]. The increase in damage intensity over the southern part of Key Biscayne (Fig. 6) was related to the northern edge of the eyewall and accompanying strong winds passing over at \approx 0835. As previously mentioned, it is apparent that the strongest damage occurred north of the center of the eye in Fig. 12 with a rapid drop-off in intensity toward the south. Indeed, Key Largo experienced minimal damage ($<$ F1) even though the eyewall passed directly overhead. Interestingly, no obvious change in the eyewall occurred even though the circulation associated with the second wind was shown to have intensified in section 2a. An aircraft reconnaissance penetrated the eye [3 km AGL (above ground level)] at \approx 0920 and did not note a significant change in the dimension of the circulation after landfall nor of the minimum surface pressure (measured by dropsonde) of \approx 931 mb (not shown).

It should be emphasized that the radar images after 0835 are from the Key West radar (range to the center

of the eye varied between 150 and 185 km). The center of the beam was approximately 2.5–3 km AGL and beam-broadening effects are severe. Even with these range limitations, it is somewhat surprising that the horizontal dimensions of the ring of convection as recorded from Key West are comparable to those seen from the Miami radar.

4. Intensification of the circulation after landfall

One of the fascinating features of the damage map shown in Fig. 2 was the apparent intensification of the tangential circulation associated with the second wind after landfall, attaining F3 intensity locally in the right-rear quadrant. Possible mechanisms are suggested in this section.

The effect of increased surface friction during landfall is to decrease the horizontal wind speed and increase the cross-isobar angle toward low pressure. This enhanced inflow increases the mean mass convergence and upward motion, and may even temporarily increase the moisture convergence, resulting in a deeper low. However, once the evaporation is reduced, the convection quickly dries out the boundary layer and the increased upward motion allows adiabatic cooling to dominate diabatic heating (Tuleya and Kurihara 1978; Anthes 1982).

It is interesting to speculate that this increase in convergence at the surface and subsequent stronger vertical motion may have resulted in the development of stronger rotational winds. The effect of reduced evaporation at the surface may not have been severe owing to Hurricane Andrew's path over the Everglade swamps. Indeed, Tuleya and Kurihara (1978) suggest that increasing surface roughness but not removing evaporation increases the storm's intensity. However, Anthes (1982) cautions that the importance of sensible heat gain or loss at the surface was not investigated in Tuleya and Kurihara's simulations so the relative importance of this effect is in doubt.

There are two complicating factors that should be addressed when considering this hypothesis. First, it is important to note the fraction of Andrew's storm circulation remaining over water (this fraction can be estimated from Fig. 10) as it made landfall over the tip of a peninsula versus other hurricanes making landfall over a continent. Accordingly, low-level trajectories reaching the heavy damage area were probably over land for a very short time so that reduced evaporation and sensible heating would have a smaller effect compared to increased surface roughness. Second, typical water depths and soil moisture contents in the

Everglades swamp may not have enough heat capacity to affect the storm's intensity.

Based on the extensive literature on end-wall vortices (e.g., Wilson and Rotunno 1986; Howells et al. 1988), it is known that increased surface friction reduces the centripetal acceleration per unit mass, but not the inward radial pressure force. In tornado simulations, this leads to an inward flow within the boundary layer bringing strong swirling air closer to the central axis than would have been possible without friction. This effect may have led to a transient intensification of the surface tangential winds within Hurricane Andrew.

Tuleya et al. (1984) have shown in their numerical simulations that there is a tendency for the position of the maximum low-level winds to shift from the right-front quadrant of the storm over water to the right-rear quadrant over land. This is consistent with the occurrence of F3 damage in the right-rear quadrant in Figs. 2 and 12.

5. Summary

A description of the destruction caused by Hurricane Andrew over southern Florida was presented. A detailed damage map based on aerial and ground surveys was characterized by several distinct features. The radius of curvature for the first wind was much larger than for the second wind, consistent with past studies of the surface flow field associated with a translating hurricane. The strongest damage intensity, based on an F-scale rating was primarily north of the eye track and was, surprisingly, associated with the second wind. This is believed to be the first time that surface wind speeds have been assessed as high as F3 for a landfall hurricane. It should be noted that, during the aerial and ground surveys, it was believed that the increased damage during the second wind may have been due in part to the uprooting and stripping of most of the trees during the first wind. Without this wind shelter effect, many structures were left exposed to the full force of the second wind. It is difficult to quantify this effect, but it may have resulted in a higher damage rating during the second wind by as much as one-half of an F number.

The damage map was superimposed on top of radar images recorded at Miami and Key West in order to document the relationship between the eyewall and approximate surface flow pattern estimated from the damage vectors. Minimal damage was noted over some areas traversed by the southern part of the eyewall and no apparent change in the eyewall accompanied the intensification of the circulation (this latter conclusion must be viewed with caution owing to the distant range from the Key West radar to the center

of the storm). It is hypothesized that increased friction and cross-isobar flow toward the low as the hurricane made landfall led to a more intense storm. The effect of reduced evaporation at the surface may have been negated by the storm's track over the Everglade swamps (although typical water depths and soil moisture contents in the Everglades swamp may not have had enough heat capacity to affect the storm's intensity). It is also possible that increased surface friction could have led to a transient intensification of the surface tangential winds similar to an end-wall vortex.

Future efforts should be made to conduct poststorm surveys, especially if it occurs near a WSR-88D (Weather Surveillance Radar). The combination of single-Doppler velocities with the damage track should provide important information on the structural changes that occur when hurricanes make landfall.

Acknowledgments. The authors wish to acknowledge Gregory S. Forbes and Nolan T. Atkins for their participation in the aerial and ground surveys and for their insightful discussions on the interpretation of the results. Richard Anthes, Robert Burpee, Greg Forbes, Robert Sheets, and two anonymous reviewers made many constructive comments on an earlier version of the manuscript. Peter Dodge provided the radar data from Miami and Chinghwang Liu processed the tapes for display purposes. This research was sponsored by the Office of the Federal Coordinator for Meteorological Research and NOAA/National Weather Service Office of Meteorology under Contract 40AANW204605 and ONR under Grant N00014-91-J-1068. Research facilities at UCLA were sponsored by NSF under Grant ATM9008683 and ATM9221951. The airborne survey was partially supported by NOAA/Office of Atmospheric Research through the efforts of Ned Ostenson.

Appendix: Source of wind speed estimates shown in Figure 2

Metro Fire Station—SW 87 Ave. and 58 St.: 58 m s⁻¹
U.S. Army Communications Center—SW 152 St. and 136 Ave.: 54+ m s⁻¹
²Private home—16201 SW 85 Ave.: 79 m s⁻¹
Private home—15028 SW 153 Court: 77 m s⁻¹
Private home—8950 SW 125 Terrace: 76 m s⁻¹
Private home—9268 SW 136 St.: 72 m s⁻¹
Sailboat—Angelfish Creek: 51 m s⁻¹
Virginia Key Water and Sewer Plant: 51 m s⁻¹
FPL Turkey Point Power Plant: 44+ m s⁻¹
FAA Tamiami Airport: 57 m s⁻¹
National Hurricane Center—1320 S. Dixie Highway: 74 m s⁻¹
Private home—19041 SW 129 Ave.: 45+ m s⁻¹
Private home—440 NW 132 Court: 42 m s⁻¹

²Calibrated in wind tunnel.

References

- Anthes, R. A., 1982: Tropical Cyclones: Their evolution, structure and effects. *Meteor. Monogr.*, **19**, No. 41, Amer. Meteor. Soc., 208 pp.
- Forbes, G. S., and R. M. Wakimoto, 1983: A concentrated outbreak of tornadoes, downbursts, and microbursts, and implications regarding vortex classifications. *Mon. Wea. Rev.*, **111**, 220–235.
- Frank, W. M., 1984: A composite analysis of the core of a mature hurricane. *Mon. Wea. Rev.*, **112**, 2401–2420.
- Fujita, T. T., 1980: In search of mesoscale windfields in landfalling hurricanes. Preprints, *13th Tech. Conf. on Hurricanes and Tropical Meteor.*, Miami Beach, Amer. Meteor. Soc., 43–57.
- , 1981: Tornadoes and downbursts in the context of generalized planetary scales. *J. Atmos. Sci.*, **38**, 1511–1534.
- , 1992: Mystery of severe storms. *WRL Research Paper No. 239*, The University of Chicago, 298 pp. [NTIS PB 92-182021]
- , G. S. Forbes, and T. A. Umenhofer, 1976: Close-up view of 20 March 1976 tornadoes: Sinking cloud tops to suction vortices. *Weatherwise*, **29**, 116–131.
- , R. M. Wakimoto, and D. J. Stiegler, 1980: Mesoscale damage patterns of Hurricane Frederic in relation to enhance SMS imagery. Preprints, *19th Conf. on Radar Meteorology*, Miami Beach, Amer. Meteor. Soc., 48–55.
- Gentry, R. C., 1983: Genesis of tornadoes associated with hurricanes. *Mon. Wea. Rev.*, **111**, 1793–1805.
- Holland, G. J., 1987: Mature structure and structure change. *A global view of tropical cyclones*. R. L. Elsberry, Ed., Naval Postgraduate School, 13–52.
- Howells, P. A. C., R. Rotunno, and R. K. Smith, 1988: A comparative study of atmospheric and laboratory-analogue numerical tornado-vortex models. *Quart. J. Roy. Meteor. Soc.*, **114**, 801–822.
- Hubert, L. F., 1955: Frictional filling of hurricanes. *Bull. Amer. Meteor. Soc.*, **36**, 440–445.
- Hughes, L. A., 1952: On the low-level wind structure of tropical storms. *J. Meteor.*, **9**, 422–428.
- Jordan, C. L., D. A. Hurt, and C. A. Lowrey, 1960: On the structure of Hurricane Daisy on 27 August 1958. *J. Meteor.*, **17**, 337–348.
- Jorgensen, D. P., 1984a: Mesoscale and convective-scale characteristics of mature hurricanes. Part I: General observations by research aircraft. *J. Atmos. Sci.*, **41**, 1268–1285.
- , 1984b: Mesoscale and convective-scale characteristics of mature hurricanes. Part II: Inner core structure of Hurricane Allen (1980). *J. Atmos. Sci.*, **41**, 1287–1311.
- Kelly, D. L., J. T. Schaeffer, R. P. McNulty, C. A. Doswell, and R. F. Abbey, 1978: An augmented tornado climatology. *Mon. Wea. Rev.*, **106**, 1172–1183.
- Marks, F. D., and R. A. Houze, 1984: Airborne Doppler radar observations in Hurricane Debby. *Bull. Amer. Meteor. Soc.*, **65**, 569–582.
- , and ———, 1987: Inner core structure of Hurricane Alicia from airborne Doppler radar observations. *J. Atmos. Sci.*, **44**, 1296–1317.
- , and J. F. Gamache, 1992: Dual-aircraft investigation of the inner core of Hurricane Norbert. Part I: Kinematic structure. *J. Atmos. Sci.*, **49**, 919–942.
- Mayfield, M., and L. Avila, 1993: Atlantic hurricanes. *Weatherwise*, **46**, 18–25.
- Maynard, R. H., 1945: Radar and weather. *J. Meteor.*, **2**, 214–226.
- McCaul, E. W., 1991: Buoyancy and shear-characteristics of hurricane-tornado environments. *Mon. Wea. Rev.*, **119**, 1954–1978.
- Miller, B. I., 1964: A study of the filling of Hurricane Donna (1960) over land. *Mon. Wea. Rev.*, **92**, 389–406.
- Minor, J. E., 1981: Wind effects of buildings. *Thunderstorms: A Social and Technological Documentary*, Vol. 1, 2d ed., E. Kessler, Ed., University of Oklahoma Press, 113–140.
- Novlan, D. J., and W. M. Gray, 1974: Hurricane-spawned tornadoes. *Mon. Wea. Rev.*, **102**, 476–488.
- Orton, R., 1970: Tornadoes associated with Hurricane Beulah on September 19–23, 1967. *Mon. Wea. Rev.*, **98**, 541–547.
- Powell, M. D., 1982: The transition of the Hurricane Frederic boundary-layer wind field from the open Gulf of Mexico to landfall. *Mon. Wea. Rev.*, **110**, 1912–1932.
- Shapiro, L. J., 1983: The asymmetric boundary layer flow under a translating hurricane. *J. Atmos. Sci.*, **40**, 1984–1998.
- Shea, D. J., and W. M. Gray, 1973: The hurricane's inner core region. I. Symmetric and asymmetric structure. *J. Atmos. Sci.*, **30**, 1544–1564.
- Tuleya, R. E., and Y. Kurihara, 1978: A numerical simulation of the landfall of tropical cyclones. *J. Atmos. Sci.*, **35**, 242–257.
- , M. A. Bender, and Y. Kurihara, 1984: A simulation study of the landfall of tropical cyclones using a movable nested-mesh model. *Mon. Wea. Rev.*, **112**, 124–136.
- Wakimoto, R. M., 1983: The West Bend, Wisconsin storm of 4 April 1981: A problem in operational meteorology. *J. Appl. Meteor.*, **22**, 181–189.
- Wexler, H., 1947: Structure of hurricanes as determined by radar. *Ann. N. Y. Acad. Sci.*, **48**, 821–844.
- Williams, J. 1993: Tracking Andrew from ground zero. *Weatherwise*, **45**, 8–12.
- Wilson, T., and R. Rotunno, 1986: Numerical simulation of a laminar end-wall vortex and boundary layer. *Phys. Fluids*, **29**, 3993–4005.

